Title

Temperature Profile Measurement From Radiofrequency Nasal Airway Reshaping Device

Authors

Abello, Eric H
Nguyen, Theodore V
Dilley, Katelyn K
et al.

Publication Date

2023-08-18

DOI

10.1002/lary.30942

The Laryngoscope

Temperature Profile Measurement From Radiofrequency Nasal Airway Reshaping Device

Eric H. Abello, MD; Theodore V. Nguyen, BS; Katelyn K. Dilley, BS; Donggyoon Hong, ME; Justin S. Kim, BS; Pranav S. Nair, BS; Benjamin F. Bitner, MD; Wangcun Jia, PhD; Brian J. F. Wong, MD, PhD

Objective: Nasal airway obstruction (NAO) is caused by various disorders including nasal valve collapse (NVC). A bipolar radiofrequency (RF) device (VivAer®, Aerin Medical, Sunnyvale, CA) has been used to treat NAO through RF heat generation to the upper lateral cartilage (ULC). The purpose of this study is to measure temperature elevations in nasal tissue, using infrared (IR) radiometry to map the spatial and temporal evolution of temperature.

Study Design: Experimental and computational.

Methods: Composite porcine nasal septum was harvested and sectioned (1 mm and 2 mm). The device was used to heat the cartilage in composite porcine septum. An IR camera (FLIR® ExaminIR, Teledyne, Wilsonville, OR) was used to image temperature on the back surface of the specimen. These data were incorporated into a heat transfer finite element model that also calculated tissue damage using Arrhenius rate process.

Results: IR temperature imaging showed peak back surface temperatures of 49.57°C and 42.21°C in 1 and 2 mm thick septums respectively. Temperature maps were generated demonstrating the temporal and spatial evolution of temperature. A finite element model generated temperature profiles with respect to time and depth. Rate process models using Arrhenius coefficients showed 30% chondrocyte death at 1 mm depth after 18 s of RF treatment.

Conclusion: The use of this device creates a thermal profile that may result in thermal injury to cartilage. Computational modeling suggests chondrocyte death extending as deep as 1.4 mm below the treatment surface. Further studies should be performed to improve dosimetry and optimize the heating process to reduce potential injury.

Key Words: Arrhenius integral, computational modeling, finite element model, nasal airway obstruction, nasal valve collapse, NOSE, RF treatment.

***Laryngoscope*, 00:1–8, 2023**

INTRODUCTION

Nasal airway obstruction (NAO) is caused by structural and inflammatory disorders of the nasal cavity that restricts normal airflow and is associated with other symptoms that can negatively impact a patients' quality of life.[1,2] Recent focus on NAO has centered on nasal valve dysfunction, specifically the internal nasal valve (INV), which is the area of greatest resistance to airflow into the nasal cavity.[3] The structures that define the INV are the cartilaginous septum medially, caudal end of the upper lateral cartilage (ULC) laterally, and the inferior turbinates forming the inferior border.[3,4] Nasal valve collapse (NVC) is a phenomenon whereby the lateral nasal wall collapses in response to air entering this narrowed region, accelerating, and causing a decrease in intraluminal pressure.[5–7] It is essential to properly diagnose and address this area for successful treatment of NAO.

Nonsurgical management of NVC includes adhesive external nasal dilator strips and internal nasal dilators. These interventions prevent lateral nasal wall collapse by mechanically dilating the nasal airway or stiffening the lateral nasal wall.[8,9] Surgical management of this area includes the precision placement of various autologous cartilage grafts or synthetic biomaterials and suturing techniques.[10–12] Given the recovery time, risks, and costs of surgery, there is a demand for less invasive treatments.

Radiofrequency (RF) heating is the application of high frequency radiation to generate heat via capacitive coupling. RF has been used for inferior turbinate reduction, which has been shown to reduce tissue volume in a precise and targeted manner.[13] Similarly, studies have demonstrated that needles delivering RF energy can be applied intranasally to the mucosa overlying the lower edge of the ULC to improve Nasal Obstruction Symptom Evaluation (NOSE) scores.[14] Although with significant patient drop-out, promising results were also demonstrated in a 4 year follow-up study, which showed stable and lasting improvement in the patients' symptoms of NAO.[15] The rationale behind the efficacy of this treatment is thought to be related to the stabilization of the INV through the creation of scar formation and retraction

From the Beckman Laser Institute and Medical Clinic (E.H.A., T.V.N., K.K.D., D.H., J.S.K., P.S.N., W.J., B.J.F.W.), Irvine, California, USA; Department of Otolaryngology – Head and Neck Surgery (E.H.A., B.F.B., B.J.F.W.), University of California – Irvine Medical Center, Orange, California, USA; and the Department of Biomedical Engineering (B.J.F.W.), Henry Samueli School of Engineering, Irvine, California, USA.

Editor's Note: This Manuscript was accepted for publication on July 19, 2023.

Triological Society Combined Sections Meeting 2023. January 26–28, 2023.

The authors have no funding, financial relationships, or conflicts of interest to disclose.

Send correspondence to Brian J. F. Wong, Department of Otolaryngology–Head and Neck Surgery, University of California, Irvine Medical Center, 101 The City Dr South, Orange, CA 92868, USA. Email: bjwong@uci.edu

DOI: 10.1002/lary.30942

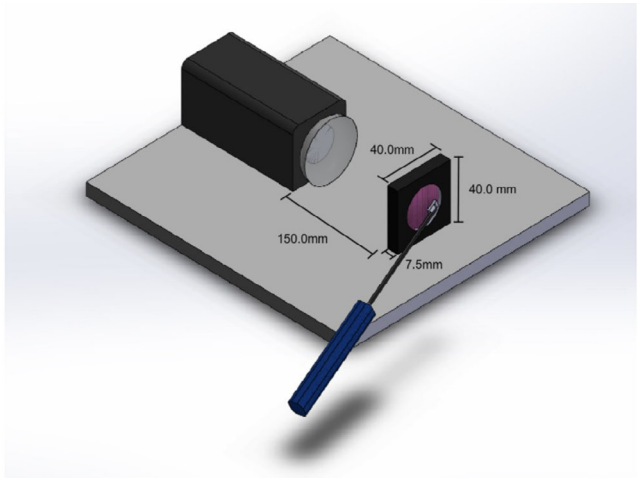

Fig. 1. General experiment setup schematics. The experimental setup was reconstructed using 3D modeling software. An IR camera was placed 150.0 mm from the tissue sample facing a 40 mm × 40 mm jig with a central cutout where samples are placed. Contralateral to the IR camera is RF treatment site. [Color figure can be viewed in the online issue, which is available at www.laryngoscope.com.]

of tissue, though human biopsy results would be the only means to directly validate this hypothesis.[16]

The biophysics of this bipolar RF device (VivAer, Aerin Medical, Mountain View, CA) as it relates to its interaction with the intended target of the ULC has not been well studied. The effect of RF energy on the relatively thin and fragile ULCs, through the thin overlying mucosa has not been explored with rigor, though this is clearly a temperature mediated effect. Prior studies have demonstrated that thermally mediated shape change of cartilage is thought to occur at a threshold of 60–75°C, when fast IR laser sources are used to generate heat, whereas the current RF device reaches a temperature of 60°C, though over *an order of magnitude longer application time*. The effects of heating cartilage for sustained periods of time using the present RF device are unknown, nor has the temperature with respect to depth distribution been modelled.[17–20] This study intends to measure surface temperature profiles, model the heating process using a finite element analysis (FEA), and then calculate tissue damage using rate process models in an effort to better understand the biophysical interactions between this device and porcine septal tissue.

METHODS

Specimen Preparation

Intact composite (cartilage with native mucosa attached) nasal septums were harvested from frozen porcine crania obtained from a local abattoir after returning to ambient temperature. The septums were then precisely sectioned by hand in a sagittal plane to produce 1 and 2 mm thick specimens to mimic human nasal cartilage with overlying mucosa. Specimen thickness was verified with a digital Vernier caliper. Mucosal thickness was also verified with a caliper and determined to be 0.5–1.0 mm. Mucosa remained natively secured on one surface, whereas the other side was the cut surface of the cartilage. Specimens were then cut into 40 × 40 mm squares and placed into 0.9% saline solution until use.

RF Heating

The samples were secured to a custom jig composed of a single stainless-steel plate (40 × 40 mm) with a 30 mm round cutout centrally (Fig. 1). This jig was placed 15 cm away from the IR camera (FLIR A310, FLIR, Wilsonville, USA).

Prior to treatment, the tissue was equilibrated to ambient temperature (20°C). The bipolar RF stylus was placed on the mucosal surface mimicking clinical use and the IR temperature was recorded from the opposite side (Fig. 1). Gentle pressure to maintain good tissue contact and a thin layer of saline gel was applied to the RF tip to ensure all eight electrodes-maintained contact with the tissue.

Temperature was recorded during heating and during re-equilibration to ambient temperatures. Per the manufacturer,

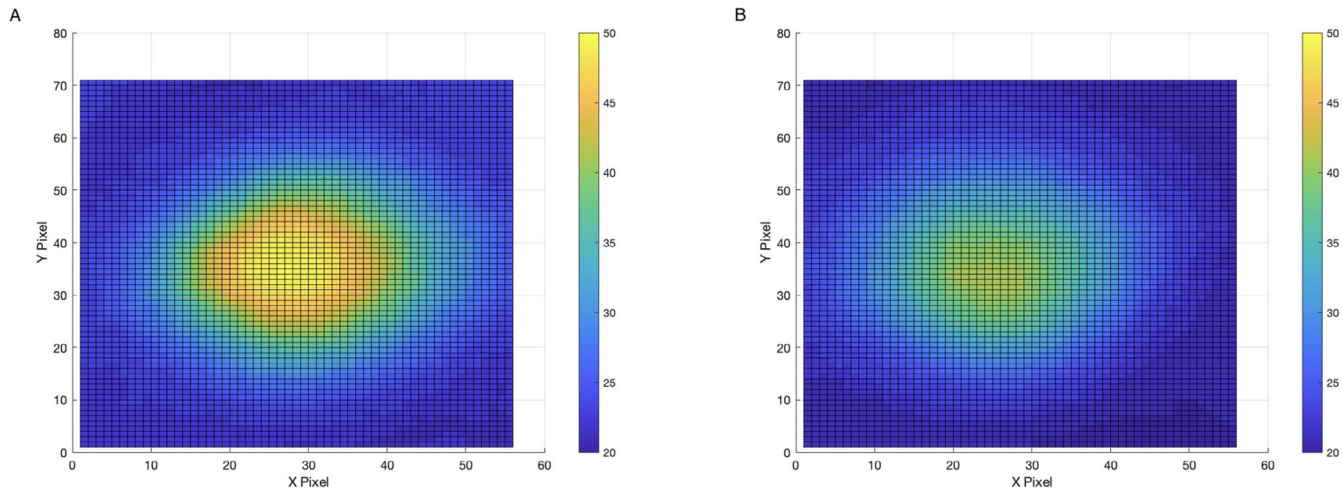

Fig. 2. 2D temperature profile of treatment. 2D temperature profile of treatment Grayscale recordings of a 60 × 80 pixel ROI from (A) 1 mm and (B) 2 mm samples were uploaded to Matlab and analyzed to find the frame where maximum temperature occurs. The figure above displays the extracted frame with each pixel's RGB value being correlated to temperature values from the thermal imaging software. Color scale was normalized between 20 and 50°C to better visualize heat dissipation within the tissue. [Color figure can be viewed in the online issue, which is available at www.laryngoscope.com.]

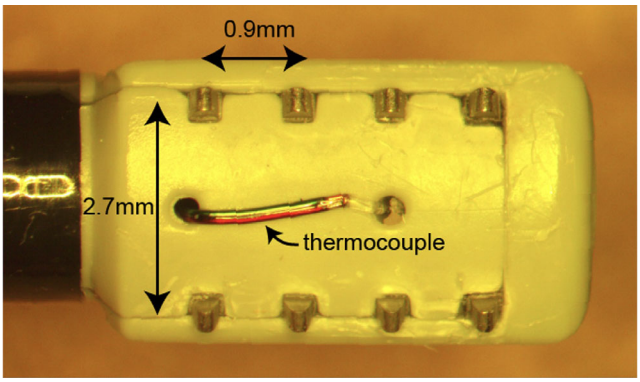

Fig. 3. Digital Image of RF Probe. (A) Digital image of RF probe surface with electrodes and thermocouple. [Color figure can be viewed in the online issue, which is available at www.laryngoscope.com.]

recommended treatment settings were: temperature of 60°C, power of 4 W, and treatment time of 18 seconds. Experimental RF heating time was over 12 s and IR temperature recordings were taken for 200 s. We chose a treatment time of 12 s as full 18 s cycles would trigger the manufacturers' single use software.

Data Processing and Analysis

The temperature (°C) with respect to time (seconds) of the region of interest (ROI) was exported from the camera for further analysis. This data was collected from a blackbody radiation source (Model BB701, Omega Engineering Inc., Stamford, CT) from 15 to 75°C. Data were analyzed via MATLAB (MathWorks, Massachusetts, USA) to generate spatial temperature profiles as a function of time (Fig. 2).

For FEM, average temperature within a 3 × 3 pixels region of interest (ROI) at the treatment center point was calculated. Similarly, the average temperature from a second 3 × 3 ROI was recorded 2.5 mm away from the center point.

Finite Element Model Analysis

FEM (ANSYS mechanical 2022 R1 package, Canonsburg, PA) was used to calculate temperature profiles with respect to time and depth, and to estimate subsurface temperature profiles. Subsurface temperature profile information is important as it will be higher than the temperature at the surface where IR measurements were recorded, and the time–temperature profile can be used to estimate tissue injury. For the heating source in FEM, the time–temperature curve was extracted from thermocouple data that is provided by the device itself. A thermocouple embedded into the device handpiece adjacent to the needle electrodes records temperature (Fig. 3A). As temperature is updated about once every second, the heating curve is discretized. The FEM was compared to the IR temperature measurements.

For the RF device probe, the eight electrodes are protruded from the probe surface in a 4 × 2 configuration with a thermocouple centrally (Fig. 3A). The 3D model was imported into ANSYS. The following initial boundary conditions were applied based on the property of porcine cartilage: mesh size 0.1 mm, density of 1100 kg/m^3, specific heat constant of 3568 J/kg°C, and thermal conductivity of 0.4783 W/m°C at 27°C, 0.5182 W/m°C at 37°C, and 0.5757 W/m°C at 50°C.[21,22] An ambient temperature and cartilage temperature of 20.5°C and a film coefficient of 280 W/m^2°C for air convection were used.[21] Cartilage was assumed to be at ambient temperature with no convection cooling occurring. Arrhenius integral formulation has been widely used in many disciplines to estimate the evolution of physical properties after exposure to a heat source. To estimate chondrocyte viability, Arrhenius integral formulation as in Equation (1) was adopted:

$$\Omega(\tau) = A\int_0^{\tau} e^{-\frac{E_a}{RT(t)}}dt, \tag{1}$$

where A (s^{-1}) is a pre-exponential constant, τ (s) the total heating time, E_a ($J{\cdot}mol^{-1}$) the activation energy, R ($J{\cdot}mol^{-1}{\cdot}K^{-1}$) the gas constant, and T (K) the absolute temperature.[21] Diaz et al. adopted Equation (1) for cartilage thermal injury case, adopting Ω (τ) as the logarithm of the initial healthy cell concentration C_0 to healthy cell concentration $C\tau$ at time τ.[23] Diaz et al. showed that Arrhenius integral equation was a proper mathematical equation to best model cell viability with respect to time at certain given temperature. They experimentally validated this equation for cell viability modelling.

$$\Omega(\tau) = ln\left\{\frac{C_0}{C_\tau}\right\} = \int_0^{\tau} k(t)dt, \text{ where } k \equiv Ae^{-\frac{E_a}{RT(t)}}. \tag{2}$$

The equation for healthy cell concentration ratio at the time τ was derived from Equation (3):

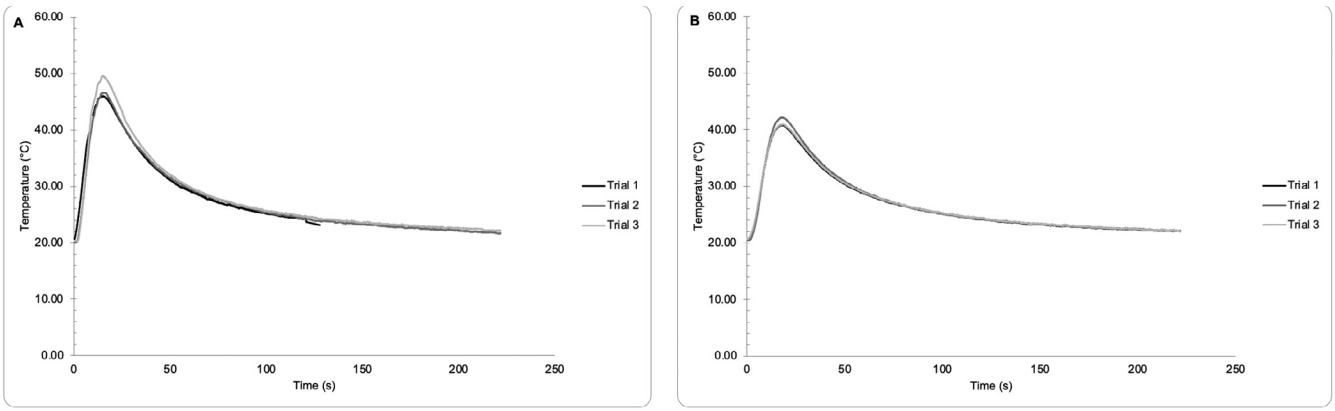

Fig. 4. Graphical representation of maximum temperature (°C) versus time (seconds) during RF energy treatment. Temperature measurements (°C) from an IR camera for (A) 1 mm ($n = 3$) and (B) 2 mm ($n = 3$) tissues were taken over 4 min (12 s treatment, 228 s cooldown) and plotted in respect to relative time (seconds).

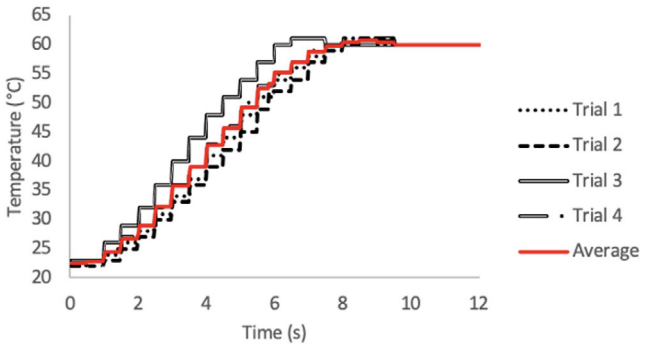

Fig. 5. Temperature versus time of experimental bipolar RF device. Temperature (°C) versus time (seconds) of RF energy treatment as reported by the device's thermocoupler. Four trials were performed and averaged before input into an FEA model. This served as a representation of RF heating during treatment. [Color figure can be viewed in the online issue, which is available at www.laryngoscope.com.]

$$\frac{C_\tau}{C_0} = \left[e^{\int_0^\tau k(t)dt} \right]^{-1}. \quad (3)$$

Healthy cell concentration after a certain period of heat treatment was determined by applying the trapezoidal rule for integration in Equation (4). Given this, the final numerical analysis equation applied in MATLAB is as follows:

$$\text{ratio}(\tau) = \left[e^{\sum_{i=1}^{n} \frac{1}{2}(k_i + k_{i-1})(t_i - t_{i-1})} \right]^{-1} (\text{where } k_0 = k_1, t_0 = 0, t_n = \tau). \quad (4)$$

Diaz *et al*. experimentally determined the coefficients of the Arrhenius equation for cartilage as follows: $A = 1.2 \times 10^{70}\ \text{s}^{-1}$ and $E_a = 4.5 \times 10^5\ \text{J·mol}^{-1}$.[23] These values were used to calculate the cell viability with respect to time in this study.

RESULTS

A total of 1 mm and 2 mm composite septal specimens were used ($n = 3$). Initial temperatures for the 1 and 2 mm samples were 20.7 ± 0.3°C and 20.7 ± 0.2°C, respectively. Peak temperatures on the mucosal side measured with the IR camera were 47.4 and 41.3°C in 1 and 2 mm samples, respectively (Fig. 4). Temperature peaked at 16.8 ± 0.7 s after initiation of treatment. After 200 s, the tissue cooled to 22.3 ± 0.2°C and 22.4 ± 0.1°C for 1

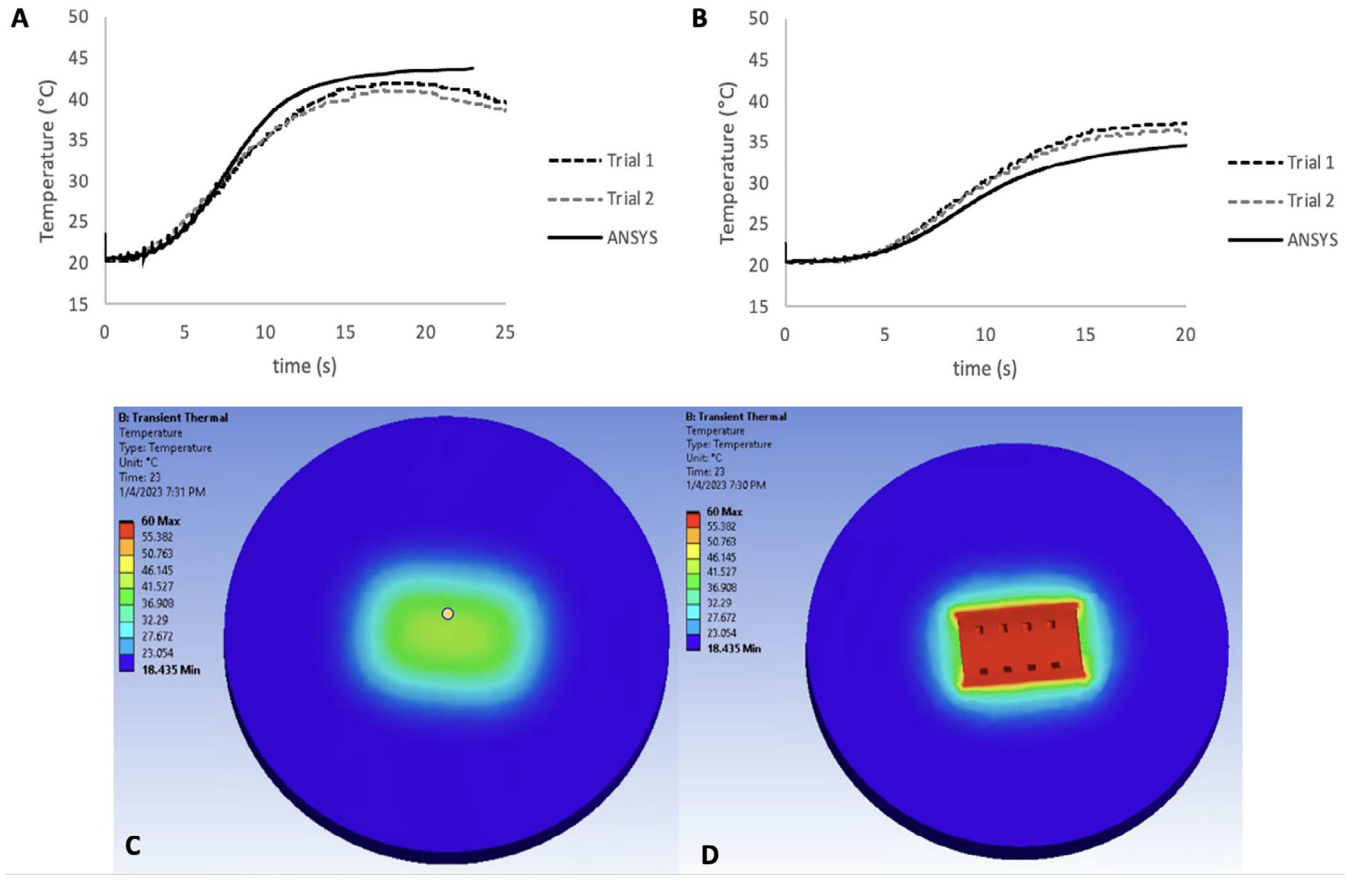

Fig. 6. Comparison between experimental results and FEA model. (A) Data Comparison at the Center of the Cartilage (2 mm Thickness) (B) Data Comparison at 2 mm away from the Center of the Cartilage (2 mm Thickness). FEA modeling of (C) IR camera side of the cartilage. Yellow marker is 2 mm away from center of probe/center of cartilage. (D) probe/mucosal side of the cartilage. Temperatures reached 41.527°C on the IR camera side of cartilage and 60°C on the probe/mucosal side. [Color figure can be viewed in the online issue, which is available at www.laryngoscope.com.]

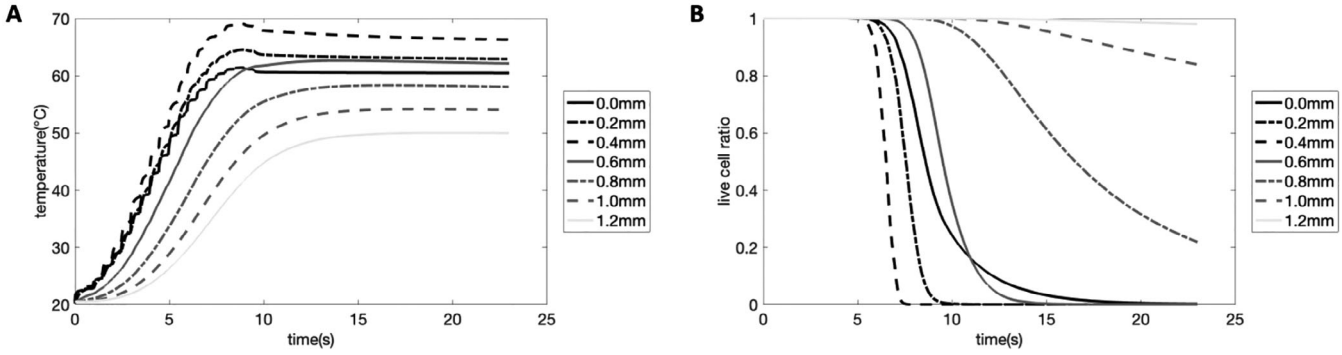

Fig. 7. FEA model verification results. (A) Temperature profile with respect to time with varying distance from the probe. (B) Live cell ratio with respect to time with varying distance from the probe.

and 2 mm, respectively. Peak temperatures were maintained for 6.6 ± 0.3 s and 10.0 ± 1.2 s for the 1 and 2 mm samples, respectively.

Finite Element Analysis

The thermocouple data (see Fig. 5) provided the temperature profile for the heat source in the FEM. Experimental results (IR temperature measurements) were compared with the results from the FEM (Fig. 6A,B). This model is an idealized model of our experimental setup with heat convection from ambient air, which served as verification of our computational model. Figure 6C,D shows the computational model of the temperature heat map after 18 s of RF heating on the probe IR camera side (Fig. 6C) and probe side (Fig. 6D). Figure 7 further analyzes the results from Figure 6 with varying depth. Figure 7A demonstrates that a temperature of 60°C was reached at a depth of 0.4 mm and 55°C was reached at a depth of 0.8 mm after 18 s of RF heating. The live cell ratio with respect to time in Figure 7B indicates that between depths of 0.0 and 0.4 mm, 100% of cells are dead after only 10 s. Beyond 0.4 mm, the cell death fraction decreases. After verification with this idealized model, anatomic conditions were applied. This computational model was performed without convective cooling to mimic the in vivo usage of the RF device against the ULC (Fig. 8A). In Figure 8B the model estimates 97.6% and 47% of chondrocytes are dead at a depth of 0.2 and 0.8 mm after 18 s of heating.

DISCUSSION

In this present study, we measured temperature during the RF heating of composite porcine septal cartilage using a commercial device designed for treating NAO. RF devices have been widely used for NAO including inferior turbinate reduction, swell body reduction, and recently for treatment of INV collapse which was recently approved by the FDA. The mechanisms of RF valve shape change for NAO are unclear but tissue retraction and volume reduction resulting in widening of the INV are espoused as mechanisms. In practice, the tip of the device is pressed against mucosa adjacent to the lower edge of the ULC and maintained in deformation until the temperature of the embedded thermocouple reaches 60°C. Then feedback control modulates energy delivery, maintaining temperature at this set point of 60°C for the duration of treatment.[14,15] The total time interval during which energy is delivered is 18 s.[14] Previous experiments exploring the effect of RF heating in cartilage have demonstrated that shape change can occur, through stress relaxation with posttreatment retention of elastic properties at temperatures similar to that reached

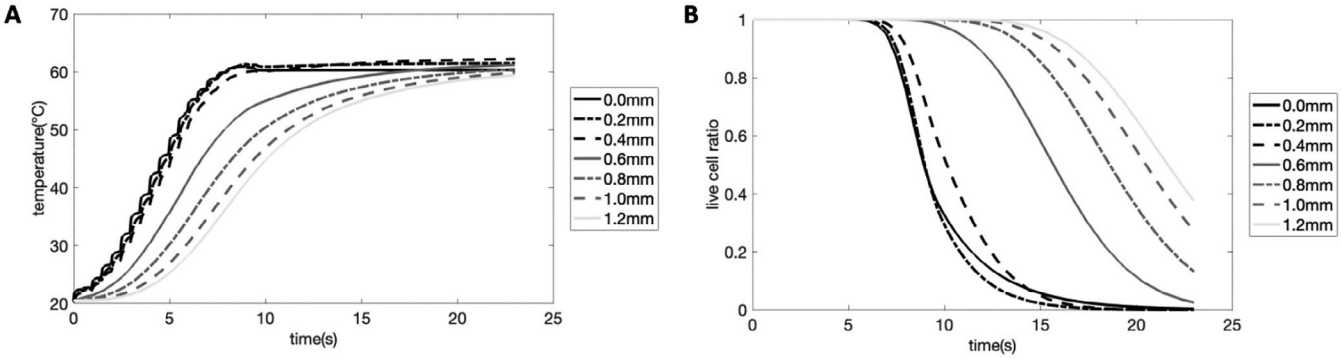

Fig. 8. *In vivo* human application simulation results. (A) Temperature profile with respect to time with varying distance from the probe. (B) Live cell ratio with respect to time with varying distance from the probe.

by the RF device.[17–20] Although multiple studies have demonstrated that there is significant improvement in subjective nasal obstructive symptoms with lasting results, its biophysical effect on the adjacent lower lateral cartilage (LLC) has yet to be studied.[14,15] In fact, one concern is whether outcomes have been followed for an adequately long time period, as devitalized cartilage could be an outcome of RF heating, but the clinical consequences may take years to appear, due simply to the long half-life of collagen type II. The present study is the first to examine this NAO treatment device using IR thermography and FEM.

Cartilage is known to undergo structural change when heated, though there is a tradeoff between shape change/stress relaxation and tissue viability. Previous studies have shown that bovine articular cartilage has a thermal damage threshold temperature of 52°C using relatively slow heating rates, beyond which chondrocytes viability is reduced.[23–25] Additional literature suggests that the storage modulus for cartilage, a measure of a material's ability to store energy elastically, decreases up to 85% when at temperatures between 50 and 65°C, allowing for shape change.[20] Damage and cellular injury do not follow any linear equation, and in fact is complex. For example, at 56°C, there was ~50% cartilage cell viability and at 60°C, there was 0% viability.[19,23,24,26–38] The temperature profile, in terms of its spatial landscape and temporal evolution, determines the extent and degree of tissue damage. For example, previous work on cartilage heating showed that 10 s of heating at 56°C produces equivalent chondrocyte death as 1 s at 62°C, this is implicit in rate process models, which were developed to study numerous thermophysical processes.[23]

Numerous studies using fast IR laser sources to generate heat, determined that at specific heating rates and temperature thresholds, stress relaxation of cartilage will occur and facilitate cartilage shape change.[19,23,24,26–38] However, thermally mediated processes in living tissues are not without risk, and heating profiles may result in few viable chondrocytes as demonstrated in the present FEM.[23] Much has been made to identify a privileged, dosimetry parameter space such that shape change can be achieved (necessary for treating NVC) with only limited cellular injury. The FEM suggests this is not entirely possible using the current device parameters, and that some degree of chondrocytes injury must occur.

IR temperature measurements were recorded from the backside of the specimen, and peak temperatures were 49.6°C and 42.2°C for the 1 mm and 2 mm samples at 12 seconds, respectively. At 2.5 mm away from the center the peak temperatures were 41.4 and 30.0°C for the 1 and 2 mm samples, respectively. This time duration of 12 s is a full 6 seconds less than what is recommended clinically, to preserve the hand stylus for further uses. A treatment time of 18 seconds would likely lead to further heating over the footprint of the device tip (2.7 mm diameter), with additional heat conduction to the periphery. As our IR temperature measurements were taken from the backside of cartilage, FEM is the only practical method to estimate the volumetric temperature distribution.

The FEM was designed to simulate the RF heating process and was compared to experimentally derived IR measurements of temperatures at two different locations (Fig. 6A,B). Parameters were then changed to simulate heating for the total duration of treatment (18 s) at different depths. The modeling demonstrated an internal temperature of 60°C at a depth of 0.6 mm, meaning tissue at this point has reached the same temperature as the source regions. The model predicts significant chondrocyte injury within the tissue volume. In addition, the modeling allowed us to quantify the decrease in concentration of healthy chondrocytes in tissue samples as a function of exposure time to different temperatures. This was made possible using the Arrhenius coefficients our laboratory previously determined in cartilage. The model predicted significant chondrocyte injury: 89.3% of chondrocytes were nonviable at a depth of 0.5 mm after 18 s of treatment, which is the manufacturer's recommended treatment duration. Even at depths of 1.0 mm, our FEM predicts 29.2% of chondrocytes were nonviable after 18 seconds of treatment. The thickness of the mucosa covering the ULC within the INV regions has not been measured or reported in any great detail, but is likely to be less than 1 mm thick here, which is less than the predicted depth of chondrocyte death.[39] Figure 7A shows the highest temperature was highest at 0.2 and 0.4 mm due to the definition of 0.0 mm as the surface of the probe. However, the heat sources are protruded out of the surface of the probe as a 3×2 configuration of prongs, which shifted the maximum temperature to 0.2–0.4 mm from the probe surface.

This is the first study to measure temperature fields produced by the current NAO treatment device and use FEM to estimate axial temperature distribution and thus calculate tissue damage. We believe the current tissue parameters used treating NAO may compromise chondrocyte viability in the treatment region. We will need to verify this using live tissue models and cellular assays as our group and others have done in the past with both electrical and optical devices. Inasmuch as patients have reported improved subjective outcomes, more rigorous objective measurements (such as INV patency) have not been studied.[14,15,40] Further studies must be performed to further evaluate the safety and efficacy of this device.

There are several limitations with this investigation. First, we performed 12 s of "active treatment" with the device held in contact with the tissue for 12 s; published device parameters specify "active treatment" duration should be 18 s with an additional 12 s of cooldown for a total of a 30 s treatment. This is much longer application time than we used, but our approach was entirely practical; handpieces are expensive and designed for single use. If used for less than 18 s, they can be reused as the single use software key is not triggered. Future studies should be performed with longer time intervals which will likely result in even more tissue injury. In addition, *ex vivo* composite porcine septum was used as human specimens without fixation are sparse and costly, particularly since these studies must be performed with fresh tissue. Fortunately, porcine tissue has been previously described as a

suitable proxy, though in the future we hope to use septal tissue from freshly euthanized rabbits.[17–19,24,29,41]

Thermal imaging recorded temperature on the opposite side of the specimen for a simple reason: the device obstructs imaging on the probe side. Hence the FEM demonstrates its value to calculate internal temperature, which was modeled using recorded measurements. We elected for a one-layer model with the tissue properties of cartilage, given the comparable thermal properties between mucosa and cartilage.[42] This simplified modeling, and for a first attempt is reasonable given thermal similarities between cartilage and mucosa which are both approximately 80% water. Previous studies have shown that cartilage and epidermis have similar thermal conductivities of 0.49 ± 0.03 and 0.37 ± 0.06 W/m/°C and heat capacities of 3568 ± 78 and 3391 ± 233 J/kg/°C, respectively. Although dermis is not mucosa, it is a soft tissue, hydrated, and collagenous in nature and likely a reasonable proxy for mucosa, hence the assumption of a one-layer model is not unrealistic. Finally, all computational models are subject to numerous assumptions and available data on tissue physical properties, as such future studies will include refinement of the FEM modeling.

Future studies will be performed to determine how RF heating affects cartilage, using confocal microscopy and live-dead assay in living cartilage tissues.

CONCLUSION

This is the first study to delineate and explore the thermal properties of a novel RF heating device used in the treatment of NAO and NVC. Using experimentally derived thermal data with further computational modeling, we determined that RF heating to the ULC creates a time–temperature threshold resulting in thermal injury and a chondrocyte death pattern dependent on cartilage depth. The significance of this amount of cellular injury is not well understood but could be expected to create unfavorable structural changes within the internal nasal valve. Further studies must be conducted using live tissue models and cellular assays to further quantify and validate the cellular damage.

BIBLIOGRAPHY

1. Rhee JS, Book DT, Burzynski M, Smith TL. Quality of life assessment in nasal airway obstruction. *The Laryngoscope*. 2003;113(7):1118-1122. https://doi.org/10.1097/00005537-200307000-00004.
2. Yamasaki A, Levesque PA, Bleier BS, et al. Improvement in nasal obstruction and quality of life after septorhinoplasty and turbinate surgery: outcomes of Septorhinoplasty and ITR. *Laryngoscope*. 2019;129(7):1554-1560. https://doi.org/10.1002/lary.27859.
3. Haight JSJ, Cole P. The site and function of the nasal valve. *The Laryngoscope*. 1983;93(1):49-55. https://doi.org/10.1288/00005537-198301000-00009.
4. Hsu DW, Suh JD. Anatomy and physiology of nasal obstruction. *Otolaryngol Clin North Am*. 2018;51(5):853-865. https://doi.org/10.1016/j.otc.2018.05.001.
5. Rhee JS, Weaver EM, Park SS, et al. Clinical consensus statement: diagnosis and management of nasal valve compromise. *Otolaryngol Neck Surg*. 2010;143(1):48-59. https://doi.org/10.1016/j.otohns.2010.04.019.
6. Cole P. The four components of the nasal valve. *Am J Rhinol*. 2003;17(2):107-110.
7. Wexler DB, Davidson TM. The nasal valve: a review of the anatomy, imaging, and physiology. *Am J Rhinol*. 2004;18(3):143-150.
8. Kirkness JP, Wheatley JR, Amis TC. Nasal airflow dynamics: mechanisms and responses associated with an external nasal dilator strip. *Eur Respir J*. 2000;15(5):929-936. https://doi.org/10.1034/j.1399-3003.2000.15e20.x.
9. Pelton RW, Peterson EA, Patel BCK, Davis K. Successful treatment of rhino-orbital mucormycosis without Exenteration: the use of multiple treatment modalities. *Ophthal Plast Reconstr Surg*. 2001;17(1):62-66. https://doi.org/10.1097/00002341-200101000-00012.
10. Khosh MM, Jen A, Honrado C, Pearlman SJ. Nasal valve reconstruction: experience in 53 consecutive patients. *Arch Facial Plast Surg*. 2004;6(3):167-171. https://doi.org/10.1001/archfaci.6.3.167.
11. Fischer H, Gubisch W. Nasal valves-importance and surgical procedures. *Facial Plast Surg*. 2006;22(4):266-280. https://doi.org/10.1055/s-2006-954845.
12. Spielmann PM, White PS, Hussain SSM. Surgical techniques for the treatment of nasal valve collapse: a systematic review. *Laryngoscope*. 2009;119(7):1281-1290. https://doi.org/10.1002/lary.20495.
13. Coste A, Yona L, Blumen M, et al. Radiofrequency is a safe and effective treatment of turbinate hypertrophy. *The Laryngoscope*. 2001;111(5):894-899. https://doi.org/10.1097/00005537-200105000-00025.
14. Jacobowitz O, Driver M, Ephrat M. In-office treatment of nasal valve obstruction using a novel, bipolar radiofrequency device. *Laryngoscope Investig Otolaryngol*. 2019;4(2):211-217. https://doi.org/10.1002/lio2.247.
15. Jacobowitz O, Ehmer D, Lanier B, Scurry W, Davis B. Long-term outcomes following repair of nasal valve collapse with temperature-controlled radiofrequency treatment for patients with nasal obstruction. *Int Forum Allergy Rhinol*. 2022;12(11):1442-1446. https://doi.org/10.1002/alr.23019.
16. Seren E. A new surgical method of dynamic nasal valve collapse. *Arch Otolaryngol Neck Surg*. 2009;135(10):1010-1014. https://doi.org/10.1001/archoto.2009.135.
17. Gaon MD, Ho KHK, Wong BJF. Measurement of the elastic modulus of porcine septal cartilage specimens following Nd: YAG laser treatment. *Lasers Med Sci*. 2003;18(3):148-153. https://doi.org/10.1007/s10103-003-0275-5.
18. Wong BJF. Stress relaxation of porcine septal cartilage during Nd:YAG (λ=1.32 μm) laser irradiation: mechanical, optical, and thermal responses. *J Biomed Opt*. 1998;3(4):409-414. https://doi.org/10.1117/1.429896.
19. Protsenko DE, Zemek A, Wong BJF. Temperature dependent change in equilibrium elastic modulus after thermally induced stress relaxation in porcine septal cartilage. *Lasers Surg Med*. 2008;40(3):202-210. https://doi.org/10.1002/lsm.20611.
20. Chae Y, Aguilar G, Lavernia EJ, Wong BJF. Characterization of temperature dependent mechanical behavior of cartilage. *Lasers Surg Med*. 2003;32(4):271-278. https://doi.org/10.1002/lsm.10167.
21. Youn JI, Telenkov SA, Kim E, et al. Optical and thermal properties of nasal septal cartilage. *Lasers Surg Med*. 2000;27(2):119-128. https://doi.org/10.1002/1096-9101(2000)27:2<119::aid-lsm3>3.0.co;2-v.
22. Pearce J, Thomsen S. Rate process analysis of thermal damage. In: Welch AJ, Van Gemert MJC, eds. *Optical-Thermal Response of Laser-Irradiated Tissue*. Springer US; 1995:561-606. https://doi.org/10.1007/978-1-4757-6092-7_17.
23. Diaz SH, Nelson JS, Wong BJF. Rate process analysis of thermal damage in cartilage. *Phys Med Biol*. 2003;48(1):19-29. https://doi.org/10.1088/0031-9155/48/1/302.
24. Diaz SH, Aguilar G, Lavernia EJ, Wong BJF. Modeling the thermal response of porcine cartilage to laser irradiation. *IEEE J Sel Top Quantum Electron*. 2001;7(6):944-951. https://doi.org/10.1109/2944.983298.
25. Diaz-Valdes SH, Aguilar G, Basu R, Lavernia EJ, Wong BJ. Modeling the thermal response of porcine cartilage to laser irradiation. In: Jacques SL, Duncan DD, Kirkpatrick SJ, Kriete A, eds; 2002:47–56. https://doi.org/10.1117/12.472507.
26. Voss JR, Lu Y, Edwards RB, Bogdanske JJ, Markel MD. Effects of thermal energy on chondrocyte viability. *Am J Vet Res*. 2006;67(10):1708-1712. https://doi.org/10.2460/ajvr.67.10.1708.
27. Edwards RB, Lu Y, Rodriguez E, Markel MD. Thermometric determination of cartilage matrix temperatures during thermal chondroplasty. *Arthrosc J Arthrosc Relat Surg*. 2002;18(4):339-346. https://doi.org/10.1053/jars.2002.29893.
28. Choi IS, Chae YS, Zemek A, Protsenko DE, Wong B. Viability of human septal cartilage after 1.45 μm diode laser irradiation. *Lasers Surg Med*. 2008;40(8):562-569. https://doi.org/10.1002/lsm.20663.
29. Zemek AJ, Protsenko DE, Wong BJF. Mechanical properties of porcine cartilage after uniform RF heating. *Lasers Surg Med*. 2012;44(7):572-579. https://doi.org/10.1002/lsm.22057.
30. Fischer R, Krebs R, Scharf HP. Cell vitality in cartilage tissue culture following excimer laser radiation: an in vitro examination. *Lasers Surg Med*. 1993;13(6):629-637. https://doi.org/10.1002/lsm.1900130607.
31. Mo JH, Kim JS, Lee JW, Chung PS, Chung YJ. Viability and regeneration of chondrocytes after laser cartilage reshaping using 1,460 nm diode laser. *Clin Exp Otorhinolaryngol*. 2013;6(2):82-89. https://doi.org/10.3342/ceo.2013.6.2.82.
32. Mainil-Varlet P, Monin D, Weiler C, et al. Quantification of laser-induced cartilage injury by confocal microscopy in an ex vivo model. *J Bone Jt Surg-Am Vol*. 2001;83(4):566-571. https://doi.org/10.2106/00004623-200104000-00012.
33. Lane JG, Amiel ME, Monosov AZ, Amiel D. Matrix assessment of the articular cartilage surface after Chondroplasty with the holmium:YAG laser. *Am J Sports Med*. 1997;25(4):560-569. https://doi.org/10.1177/03635465970250042 1.

34. Karam AM, Protsenko DE, Li C, et al. Long-term viability and mechanical behavior following laser cartilage reshaping. *Arch Facial Plast Surg*. 2006;8(2):105-116. https://doi.org/10.1001/archfaci.8.2.105.
35. Jones N, Sviridov A, Sobol E, Omelchenko A, Lowe J. A prospective randomised study of laser reshaping of cartilage In vivo. *Lasers Med Sci*. 2001;16(4):284-290. https://doi.org/10.1007/PL00011365.
36. Athanasiou KA, Fischer R, Niederauer GG, Puhl W. Effects of excimer laser on healing of articular cartilage in rabbits. *J Orthop Res*. 1995;13(4):483-494. https://doi.org/10.1002/jor.1100130403.
37. Lu Y, Edwards RB, Kalscheur VL, Nho S, Cole BJ, Markel MD. Effect of bipolar radiofrequency energy on human articular cartilage. *Arthrosc J Arthrosc Relat Surg*. 2001;17(2):117-123. https://doi.org/10.1053/jars.2001.21903.
38. Schultz RJ, Krishnamurthy S, Thelmo W, Rodriguez JE, Harvey G. Effects of varying intensities of laser energy on articular cartilage: a preliminary study. *Lasers Surg Med*. 1985;5(6):577-588. https://doi.org/10.1002/lsm.1900050606.
39. Beule AG. Physiology and pathophysiology of respiratory mucosa of the nose and the paranasal sinuses. *GMS Curr Top Otorhinolaryngol Head Neck Surg*. 2010;9:Doc07. https://doi.org/10.3205/CTO000071.
40. Brehmer D, Bodlaj R, Gerhards F. A prospective, non-randomized evaluation of a novel low energy radiofrequency treatment for nasal obstruction and snoring. *Eur Arch Otorhinolaryngol*. 2019;276(4):1039-1047. https://doi.org/10.1007/s00405-018-05270-y.
41. Wong BJF, Chao KKH, Kim HK, et al. The porcine and lagomorph septal cartilages: models for tissue engineering and morphologic cartilage research. *Am J Rhinol*. 2001;15(2):109-116. https://doi.org/10.2500/105065801781543790.
42. IT'IS Foundation. Tissue Properties Database V4.1. Published online 2022. https://doi.org/10.13099/VIP21000-04-1.